PAPER

The influence of the voltage rise rate on the breakdown of an atmospheric pressure helium nanosecond parallel-plate discharge

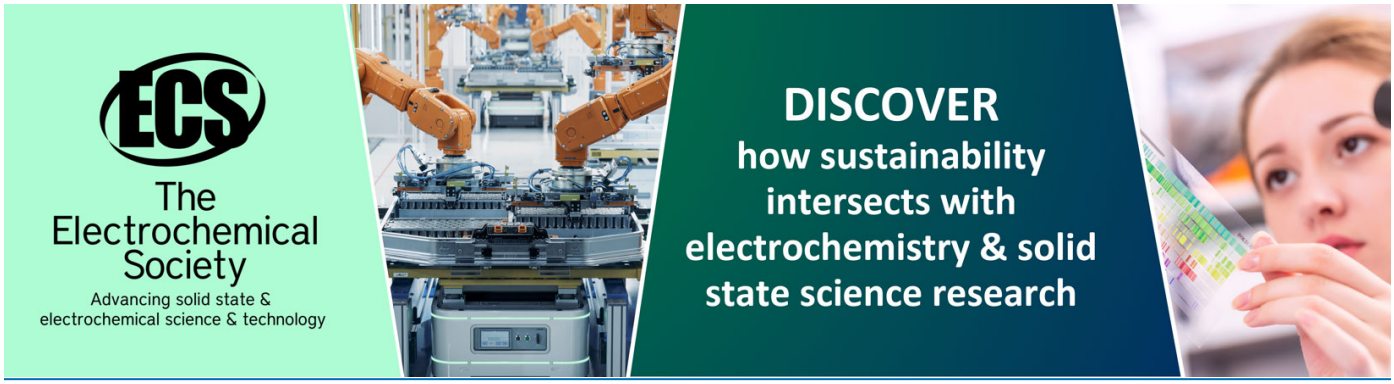

IOP Publishing Journal of Physics D: Applied Physics
J. Phys. D: Appl. Phys. **48** (2015) 125202 (10pp) doi:10.1088/0022-3727/48/12/125202

The influence of the voltage rise rate on the breakdown of an atmospheric pressure helium nanosecond parallel-plate discharge

Bang-Dou Huang[1], Keisuke Takashima[2], Xi-Ming Zhu[3] and Yi-Kang Pu[1]

[1] Department of Engineering Physics, Tsinghua University, Beijing 100084, Peoples' Republic of China
[2] Department of Electronic Engineering, Tohoku University 6-6-05 Aoba Aramaki, Aoba-ku, Sendai, MIYAGI 980-8579, Japan
[3] Institute for Plasma and Atomic Physics, Ruhr-University Bochum, Bochum 44780, Germany

E-mail: hbangdou@gmail.com

Received 5 December 2014, revised 2 February 2015
Accepted for publication 10 February 2015
Published 5 March 2015

Abstract

The influence of the voltage rise rate on a nanosecond discharge in atmospheric pressure helium is investigated. The experiment is performed with a parallel-plate discharge configuration. The voltage rise rate is varied between 0.17 kV ns^{-1} and 0.42 kV ns^{-1}. It is found that the rise rate of both the discharge current and the emission intensity increases drastically with the voltage rise rate. This demonstrates the remarkable capability of generating high energy electrons in the discharges with a high voltage rise rate. These arguments are supported by the increase in the measured effective electron temperature during the breakdown processes, namely ~18 eV when dV/dt is ~0.17 kV ns^{-1} and ~33 eV when dV/dt is ~0.42 kV ns^{-1}. Furthermore, a higher voltage rise rate results in a shorter rise time of both the discharge current and the emission intensity. Since the breakdown process evolves in the form of a cathode directed ionization wave, a shorter rise time indicates faster propagation of the ionization wave. In addition, a simple fluid model is proposed and its predicted results agree reasonably well with the important discharge parameters measured in the experiment, such as the breakdown voltage, the rise rate and rise time of the discharge current.

Keywords: voltage rise rate, breakdown, nanosecond discharge

(Some figures may appear in colour only in the online journal)

1. Introduction

The nanosecond pulsed discharges have potential application in the fields of plasma assisted ignition and combustion [1, 2], flow control [3, 4], light sources [5, 6], and material processing [7, 8]. One important advantage of the nanosecond pulsed discharges is the ability to generate a large number of high energy electrons, especially during the breakdown process under atmospheric pressure. This leads to the effective production of the active species, which are important in the applications.

The breakdown process of nanosecond discharges is influenced by many factors, including the electrode geometry [9], the initial condition (the memory effect) [10, 11], and the voltage rise rate [12, 13]. Among these factors, the voltage rise rate (dV/dt) may be the most important parameter. This is because at atmospheric pressure, the voltage rise rate critically influences the electron dynamics and provides an option for manipulating the electron energy distribution, especially in the breakdown process. When the voltage rise rate is high, high energy electrons (tens of eV) and even runaway electrons (hundreds of eV) can be generated. The effect of high energy electrons is characterized by the high discharge current, intense optical emission, and fast propagation of the streamers [14, 15]. Another phenomenon associated with the voltage rise rate is the presence of overvoltage. Under the influence of high overvoltage, the duration of the breakdown process can be drastically reduced, with a characteristic time of nanoseconds and even a sub-nanosecond [16, 17].

In this work, the discharges are generated by the high voltage pulses, and the influence of the voltage rise rate to

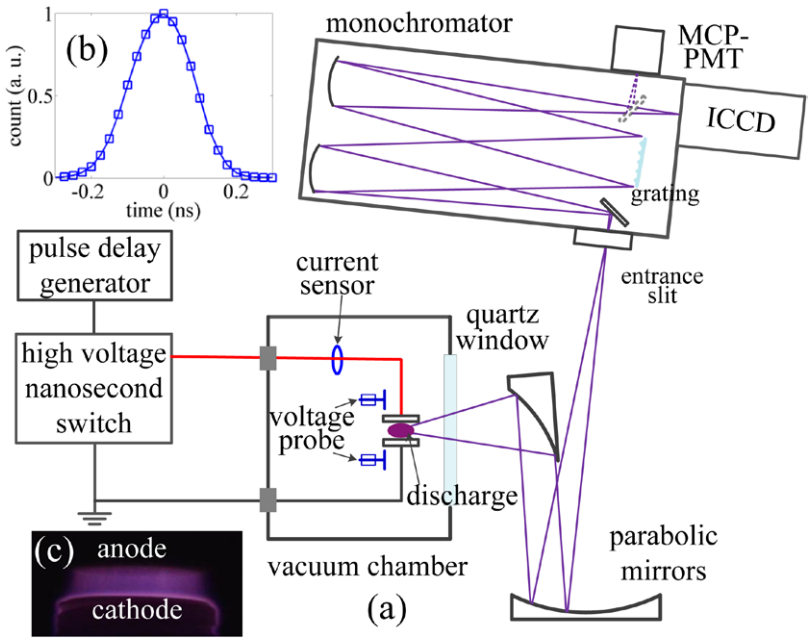

Figure 1. (*a*) The experimental setup. (*b*) An illustration for the distribution of the time when the current reaches its half maximum on the rising edge. (*c*) A typical photograph of the discharge.

discharge parameters during the breakdown process is investigated. The measured parameters include the voltage and current waveforms, the temporal evolution of the discharge image, and the emission intensity from both the helium atom and ion lines. It is found that a higher voltage rise rate leads to a higher effective electron temperature during the breakdown process, which results in more intense ionization and excitation, characterized by the larger rise rate of the discharge current and the emission intensity.

2. Experiment

Figure 1 shows the schematic of the experimental setup. A homemade nanosecond pulser is used to generate a uniform discharge between the electrodes with the atmospheric pressure helium. Pulse outputs with a different voltage rise rate can be obtained by applying different voltage to the MOSFETs, which are the key components for the switch. The pulser can produce a peak voltage up to ~7 kV with a maximum rise rate of ~0.5 kV ns^{-1}. The electrodes are two parallel plates (SUS304) with a diameter of ~4 mm and a gap of ~1 mm. The repetition frequency of the discharge is 5 kHz.

The voltage waveform is measured differentially with two capacitive voltage dividers and the current waveform is measured by a shunt current probe [11].The signal from both the voltage and current probes is recorded with an oscilloscope (LeCroy 104MXi-A).

The optical emission from the discharge is collected by an imaging system, which consists of two parabolic mirrors, a monochromator, a multichannel plate PMT (MCP-PMT, Nanjing Electronic Devices Institute, GDB-603), and an intensified charge-coupled display (ICCD) camera (PI Max 4). The MCP-PMT works in the photon counting mode and it is synchronized with the discharge current signal. The spectral response of the entire system is calibrated with a tungsten halogen lamp (Newport, 63355). The ICCD camera (without the monochromator) is used to take the image of the discharge.

In order to obtain high temporal resolution in the optical emission measurement, the jitter of the discharges should be small. The stability of the discharge is illustrated by the distribution of the time when the current reaches its half maximum on the rising edge, as shown in figure 1(*b*). The full width at half maximum of this distribution is below 0.2 ns. This ensures the temporal resolution of ~0.2 ns of the optical emission measurement, so that it is possible to capture the crucial features of the breakdown process. A more detailed description of the experimental setup can be found in [11, 18]. Figure 2(*c*) shows a photograph of the discharge, taken by a camera (Nikon D3200). It can be seen that the discharge is uniform in the direction parallel to the electrodes.

3. Modeling

Taking advantage of the parallel-plate geometry, a one-dimensional (1D) two-fluid plasma model in drift-diffusion approximation is proposed [19–21]. The purpose of this model is to have a quantitative estimate of the effect of voltage rise rate on the discharge parameters during the breakdown phase.

In this work, it is assumed that the discharge is uniform in the radial direction. This 1D model attempts to describe the evolution of the discharge in the axial direction. In addition, the model assumes the local relation between the electron mobility and diffusion coefficient with the electric field.

The governing equations are:

the electron continuity equation,

$$\frac{\partial n_e}{\partial t} = -\frac{\partial \boldsymbol{\Gamma}_e}{\partial x} + S_e \tag{1}$$

the drift-diffusion equation,

$$\boldsymbol{\Gamma}_e = -\mu_e n_e \boldsymbol{E} - D_e \nabla n_e \tag{2}$$

the electron energy conservation equation,

$$\frac{\partial(n_e\varepsilon_e)}{\partial t} = -\frac{\partial \boldsymbol{\Gamma}_{e\varepsilon}}{\partial x} - \boldsymbol{\Gamma}_e \cdot \boldsymbol{E} + Q_\varepsilon \tag{3}$$

where,

$$\boldsymbol{\Gamma}_{e\varepsilon} = -\mu_e n_e \varepsilon_e \boldsymbol{E} - D_e \nabla (n_e\varepsilon_e) = \varepsilon_e \boldsymbol{\Gamma}_e - n_e D_e \nabla \varepsilon_e \tag{4}$$

and

$$Q_\varepsilon = -\frac{3m_e}{M_i}\nu_m(T_e - T_g) - \sum \Delta\varepsilon_{\text{inel},i}\nu_{\text{inel},i} \tag{5}$$

the ion continuity equation,

$$\frac{\partial n_i}{\partial t} = -\frac{\partial \boldsymbol{\Gamma}_i}{\partial x} + S_e \tag{6}$$

where,

$$\boldsymbol{\Gamma}_i = \mu_i n_i \boldsymbol{E} - D_i \nabla n_i \tag{7}$$

The source term for the electron–ion pair is expressed as,

$$S_e = n_e\, n_g\, Q_{ion} \tag{8}$$

As this model only covers the discharge evolution during the breakdown period, the recombination and stepwise ionization processes can be omitted as their contribution is much weaker than the ground state ionization [19].

The electric potential and field is obtained from the Poisson equation,

$$\frac{\partial^2 V}{\partial x^2} = -\frac{\partial \boldsymbol{E}}{\partial x} = -\frac{e}{\epsilon_0}(n_i - n_e) \tag{9}$$

In the above equations, n_e is the electron density. $\boldsymbol{\Gamma}_e$ is the electron flux. $\boldsymbol{E}$ is the electric field. μ_e is the electron mobility and D_e is the electron diffusion coefficient. μ_e and D_e are obtained from the solution of the Boltzmann equation by Bolsig+ [22, 23]. ε_e is the electron mean energy. $\boldsymbol{\Gamma}_{e\varepsilon}$ is the electron energy flux. Q_ε is the total electron energy production (and loss) rate. m_e and $M_i$are the mass of electron and ion, respectively. ν_m is the electron momentum transfer frequency. T_e and T_g are the electron temperature and gas temperature, respectively. $\nu_{\text{inel},i}$ is the ith inelastic collision frequency and $\Delta\varepsilon_{\text{inel},i}$ is the energy loss in the ith inelastic collision. n_i is the ion density. $\boldsymbol{\Gamma}_i$ is the ion flux. μ_i is the ion mobility and D_i is the ion diffusion coefficient. Q_{ion} is the ionization rate coefficient. e is the electron charge and ϵ_0 is the vacuum permittivity.

For the electrons, its flux at the boundary is contributed by the diffusion, drift, and secondary electron emission due to the impact of the ions. For the ions, the flux at the boundary is contributed by the diffusion and the drift under the electric field [21]. Therefore, the boundary conditions are written as:

for the cathode (at 0 mm),

$$\boldsymbol{\Gamma}_e = -\gamma \boldsymbol{\Gamma}_i\ (\text{if } \boldsymbol{\Gamma}_i < 0) - \frac{1}{4} n_e v_{\text{eth}} - u_e n_e |\boldsymbol{E_c}|\,(\text{if } \boldsymbol{E_c} > 0) \tag{10}$$

$$\boldsymbol{\Gamma}_{e\varepsilon} = -\gamma \boldsymbol{\Gamma}_i \varepsilon_{se} (\text{if } \boldsymbol{\Gamma}_i < 0) - \frac{1}{4} n_e v_{\text{eth}} \varepsilon_e - u_e n_e \varepsilon_e |\boldsymbol{E_c}|\,(\text{if } \boldsymbol{E_c} > 0), \tag{11}$$

$$\boldsymbol{\Gamma}_i = -\frac{1}{4} n_i v_{\text{ith}} - u_i n_i |\boldsymbol{E_c}|\,(\text{if } \boldsymbol{E_c} < 0) \tag{12}$$

for the anode (at d = 1 mm),

$$\boldsymbol{\Gamma}_e = -\gamma \boldsymbol{\Gamma}_i\ (\text{if } \boldsymbol{\Gamma}_i > 0) + \frac{1}{4} n_e v_{\text{eth}} + u_e n_e \left| \boldsymbol{E_a} \right| \left(\text{if } \boldsymbol{E_a} < 0\right), \tag{13}$$

$$\boldsymbol{\Gamma}_{e\varepsilon} = -\gamma \boldsymbol{\Gamma}_i \varepsilon_{se} (\text{if } \boldsymbol{\Gamma}_i > 0) + \frac{1}{4} n_e v_{\text{eth}} \varepsilon_e + u_e n_e \varepsilon_e \left| \boldsymbol{E_a} \right| (\text{if } \boldsymbol{E_a} < 0), \tag{14}$$

$$\boldsymbol{\Gamma}_i = \frac{1}{4} n_i v_{\text{ith}} + u_i n_i |\boldsymbol{E_a}|\,(\text{if } \boldsymbol{E_a} > 0) \tag{15}$$

where γ is the secondary electron emission coefficient (which is taken as 0.1), v_{eth} is the electron thermal velocity, $v_{\text{ith}}$is the ion thermal velocity, and ε_{se} is the energy of the secondary electrons (assumed to be ~1 eV [20]). $\boldsymbol{E_c}$ and $\boldsymbol{E_a}$ are the electric field at the cathode and anode, respectively.

The voltage on the cathode (ground electrode) is 0 V and the voltage on the anode (high voltage electrode) V_a is:

$$V_a = V_s - I_{\text{dis}} \times R_s \tag{16}$$

where V_s is the output voltage from the pulser and R_s is the internal resistance of the pulser (~220 Ω). I_{dis} is the discharge current and it is given by:

$$I_{\text{dis}} = e \times \frac{S}{d} \int_0^d (\boldsymbol{\Gamma}_i - \boldsymbol{\Gamma}_e)\mathrm{d}x \tag{17}$$

where S is the area of the electrode and d is the distance between the electrodes.

4. Results and discussions

4.1. The evolution of the discharge

Figure 2(a) shows the measured waveform of voltage for the discharge with three different values of dV/dt. When the dV/dt is ~0.42 kV ns^{-1}, the breakdown starts at ~0 ns with a breakdown voltage of ~2.6 kV, while for the case of dV/dt ~0.17 kV ns^{-1}, the breakdown begins at ~4 ns with a breakdown voltage of ~1.8 kV. The phenomenon that a larger dV/dt leads to an earlier breakdown and a higher breakdown voltage can be explained by the 'breakdown delay' theory [16, 24]. This theory assumes that the breakdown happens when the electric field generated by the space charge is comparable with the external electric field. In the pre-breakdown phase (dark regime), the electrons multiply and the space charge develops with the increase of external voltage. At a given time, when the dV/dt is larger, the rate of the electron multiplication and space charge development is faster, due to the existence of more high energy electrons generated by higher external voltage. Therefore, the breakdown tends to happen earlier. Even so, the external voltage at the time when breakdown occurs is still

higher due to the higher voltage rise rate (~2.6 kV when dV/dt is ~0.42 kV ns^{-1} versus ~1.8 kV when dV/dt is ~0.17 kV ns^{-1}). In addition, a relationship between the breakdown voltage and the voltage rise rate developed by a breakdown model in [24] is shown in figure 7. Even though the value of the breakdown voltage has some difference, the model result and the experimental data do have the same trend.

Another feature in figure 2(a) is the existence of a small dip in the voltage waveform after the breakdown happens. This is because the rise of the voltage is disturbed by the surge in the discharge current during the breakdown. A similar result has been observed in [25]. The continuous growth of the current eventually leads to the decay of the voltage across the electrodes due to the internal resistance of the pulser.

In the same fashion, figure 2(b) shows the measured waveform of the discharge current, obtained by subtracting the displacement current from the total current. Figure 2(c) shows a close-up view of the current waveform between −2 ns and 10 ns. When dV/dt is ~0.42 kV ns^{-1}, the current has an exponential growth during ~0–1 ns, while for the case of dV/dt ~ 0.17 kV ns^{-1}, it takes much longer for the current to reach its first peak (~4–8 ns), when the breakdown process ends. Even though the current has an exponential growth during the breakdown phase in all three cases, the discharge with the largest dV/dt has the highest rate of current increase. This is caused by the stronger electron multiplication produced by a larger number of high energy electrons (with energies >24.6 eV) during the breakdown process. The high current is an indication of the existence of an anisotropic part in the electron velocity distribution function (EVDF) due to the strong field. This anisotropy is more pronounced in the high dV/dt case. In addition, when dV/dt is larger, the current rise time is shorter (~1.8 ns when dV/dt is ~0.17 kV ns^{-1} versus ~0.5 ns when dV/dt is ~0.42 kV ns^{-1}). In fact, the build-up time of the discharge channel predicted by the fluid model decreases from ~1.9 ns to ~0.6 ns (not shown), which is consistent with the measured rise time. A shorter rise time indicates a faster build-up of the discharge channel. This has been interpreted as the result of a faster ionization wave under a more intense field in the wave front [26].

The voltage and current waveform from the model for the corresponding values of dV/dt are also shown with the dash lines in figures 2(a) and (c). It is interesting that this simple fluid model can capture the same features observed in the experiment: a larger dV/dt leads to an earlier breakdown, a higher breakdown voltage, a higher current rise rate, and a shorter current rise time. However, such a simple and crude fluid model cannot produce a quantitative agreement with the experimental data. For example, the model underestimates the current rise rate by ~50%. One of the reasons is that the fluid model underestimates the ionization rate since the real electron energy distribution function (EEDF) may have an enhanced high energy tail [13, 27]. In addition, the drift-diffusion approximation cannot account for the non-local effect, which is significant under the well-enhanced electric field in the ionization wave front. This field enhancement effect is further intensified by the electrons running away from the wave front (non-local effect), which increases the space charge

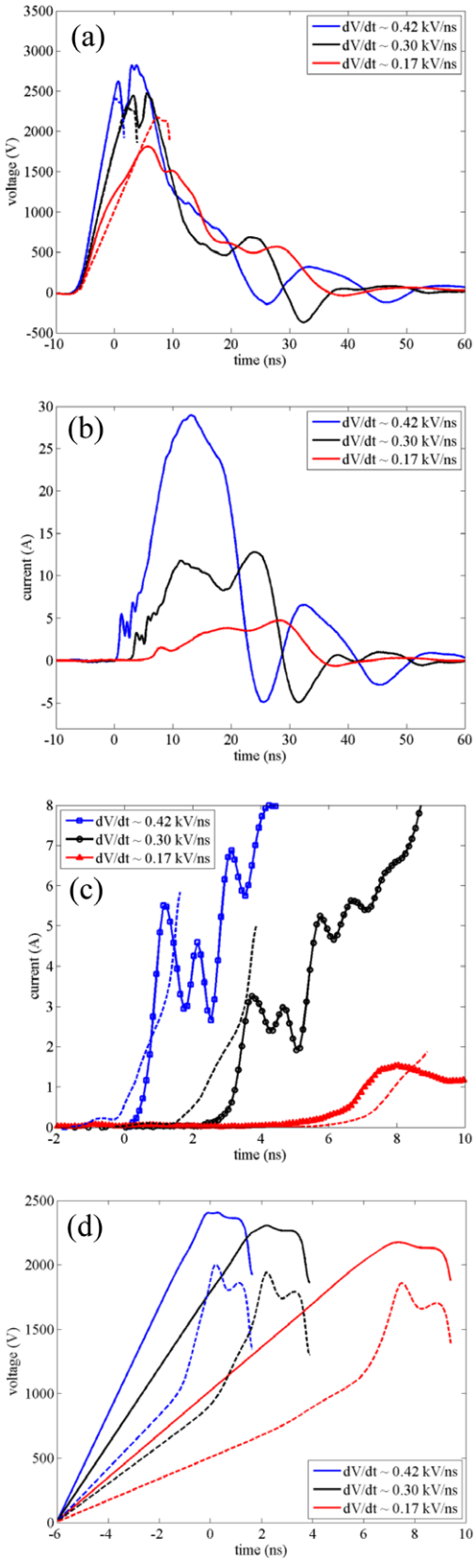

Figure 2. The voltage (a) and the current (b) waveform with different values of dV/dt; (c) is a close-up of the current waveform during −2 ns to 10 ns. The dash lines are the voltage and current waveform obtained from the simple fluid model. Figure 2(d) shows the evolution of the voltage at the anode (solid lines) and at the middle point of the electrodes (dash lines) from the model.

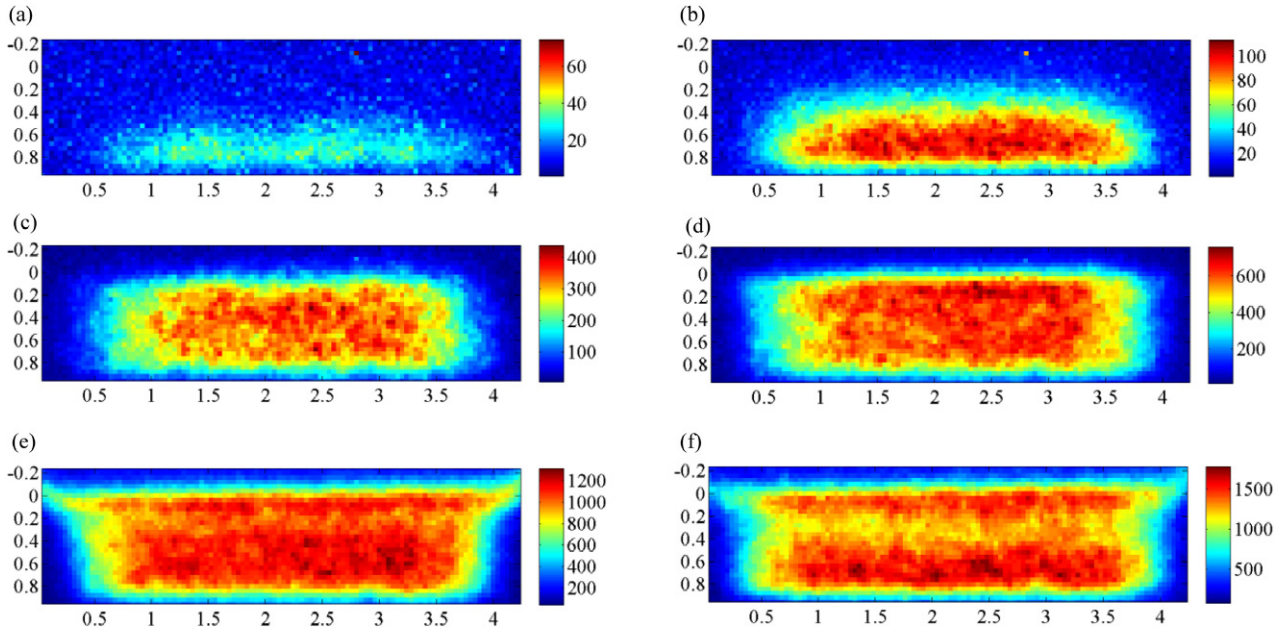

Figure 3. A two-dimensional image of the discharge evolution in dV/dt ~ 0.17 kV ns^{-1} case. The cathode is at ~0 mm and the anode is at ~1 mm in the vertical direction.

density and the propagation speed [19, 28]. This may be another reason why the model predicts a slower rise rate and a longer rise time for the current, compared with the measured values.

Figure 2(*d*) shows the voltage waveform at the anode (V_a) and at the middle point between the electrodes (V_m) obtained from the model. The same set of values for the dV/dt is used as that in figure 2(*a*). It can been seen that before the breakdown, V_m rises in proportion with V_a, which indicates the field is hardly distorted and the effect of the space charge is insignificant. However, when the breakdown happens, there is an abrupt change in the rise rate of V_m. This is due to the field enhancement effect in the ionization wave front when the breakdown happens. When the ionization wave is propagating, the electric field in the wave front is enhanced while the field behind the wave front is relatively weak. Therefore, when the ionization wave passes by a given point, the potential at this point is significantly elevated. Notice that this effect is stronger in the larger dV/dt case, which is confirmed by the faster rise rate of V_m. This effect will intensify the generation of high energy electrons during the breakdown process.

Figure 3 shows the temporal evolution of the discharge image when dV/dt is ~0.17 kV ns^{-1}. The cathode is at ~0 mm and the anode is at ~1 mm. It can be seen that the discharge is quite uniform in the direction parallel to the electrode at any given time.

At the beginning of the breakdown (~4–4.5 ns), the emission first appears near the anode (figure 3(*a*)). During this time, the electrons are multiplied and accelerated from the cathode to the anode under the influence of the external field, a typical characteristic of the Townsend regime. Later on (~4.5–6 ns), the bright region expands toward the cathode, along with an increase in the intensity (figures 3(*b*)–(*d*)). These figures show the signature of a cathode directed ionization wave, with a speed of ~0.5 mm ns^{-1}. During this period, the current is relatively low and the voltage across the discharge is still high (figures 2(*a*) and (*b*)). This feature is similar to the first (primary) streamer observed in atmospheric pressure pin-to-plate and rod-to-cylinder discharges, reported in [29, 30], which also propagates from the anode to the cathode.

After the discharge channel has been formed, a sandwich structure appears, with one dark region between two bright regions (figures 3(*e*) and (*f*)). This is the typical feature of a glow discharge, i. e. the formation of a cathode sheath region and a positive column region [29–31]. The emission intensity continuously increases during this period, as well as the current (figure 2(*b*)). The voltage across the discharge drops due to the increase of the current and the internal resistance of the pulser. However, there is no secondary streamer observed. One possible reason is the small gap distance (~1 mm) in this experiment. This can have two effects on the observation of the secondary streamer. (1) The speed of the secondary streamer can be the order of 1 cm ns^{-1} [14, 30, 32], which is too fast to be observed with our ICCD (minimum gate width ~0.5 ns). (2) The scale length of the secondary streamer (~1 mm) is comparable to the gap between the electrodes. Compared with the discharges reported in [29, 30], our discharge has a high repetition rate (5 kHz). This may lead to a strong memory effect and relatively high electron density after the first (primary) streamer. In this case, the continuous increase of the ionization rate happens simultaneously in the volume between the electrodes, which tends to diminish the feature associated with the propagation of the secondary streamer.

In fact, the simple fluid model can also give the same picture on the development of the discharge pattern. In order to compare with the experimental observation of the discharge development in figure 3, figure 4 shows the temporal evolution of the electric field profile (*a*), the space charge density distribution (*b*), and the electron density profile (*c*) obtained from the fluid model, when dV/dt is ~0.17 kV ns^{-1}.

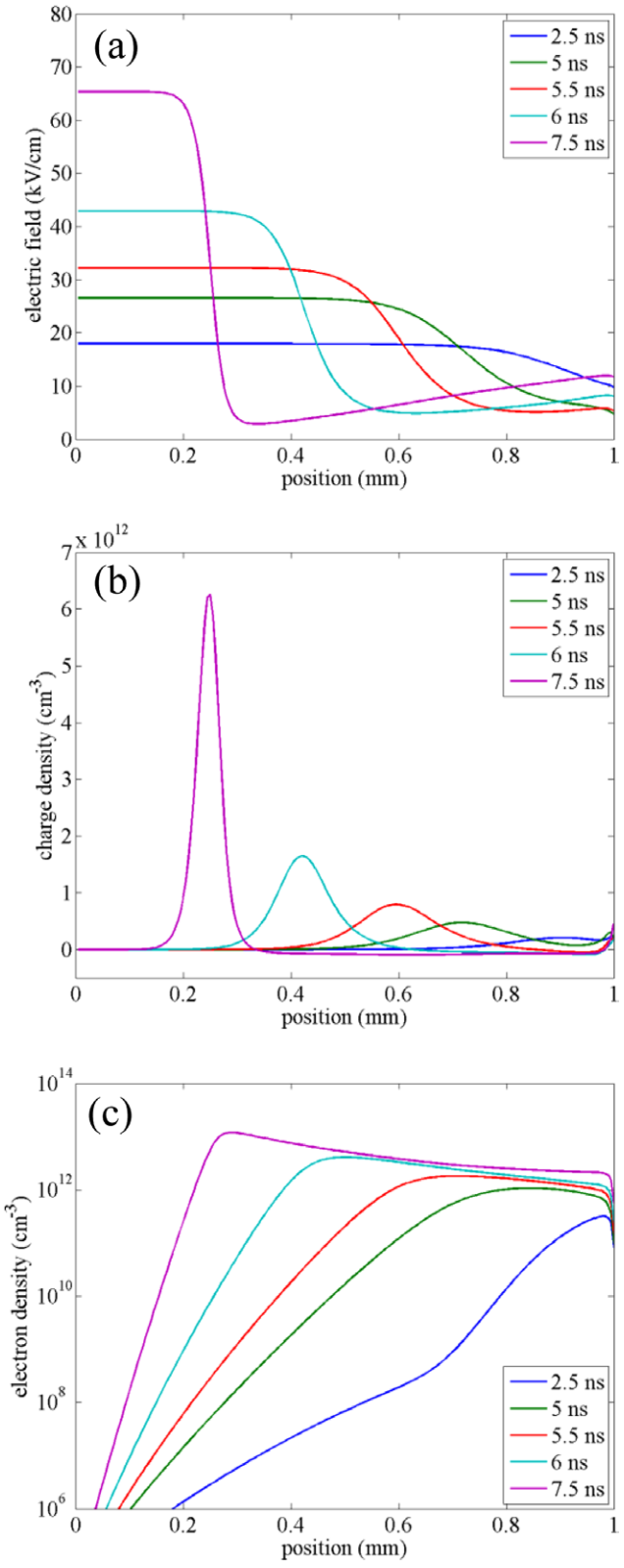

Figure 4. The evolution of the electric field (*a*), the space charge density (*b*), and the electron density (*c*), obtained from the fluid model in d*V*/d*t* ~ 0.17 kV ns^{-1} case.

It can be seen that at the very beginning of the discharge (2.5 ns), the electric field is almost uniform between the electrodes (figure 4(*a*)) and the space charge density is low (figure 4(*b*)). The electrons multiply from the cathode to the anode, forming an exponential-like distribution (figure 4(*c*)). At the same time, the space charge accumulates near the anode and distorts the electric field, with a net effect of enhancing the electric field near the cathode and weakening that near the anode. This initializes the propagation of a cathode directed ionization wave, which can be clearly identified by the movement of the peak of the charge density from the anode to the cathode. The same feature can be seen from the evolution of the discharge image (figure 3). As reported by the simulation results in [19, 23], the electric field in front of the ionization wave is enhanced, while that behind the wave is weakened. Meanwhile, the electron density continuously increases due to ionization.

For higher d*V*/d*t* cases, the model predicts a similar sequence of the discharge development in the breakdown process, but over a much shorter time scale. In these cases, the build-up time of the discharge channel is too short to obtain the temporal evolution of the discharge images, due to the limited gate width of the ICCD (~0.5 ns).

4.2. The evolution of the emission intensity from the helium atom and ion lines

Figure 5(*a*) shows the temporal evolution of the He I 667.8 nm line (helium atom $3^1D \rightarrow 2^1P$). It can be seen that, during the breakdown process, this emission intensity increases exponentially by more than two orders of magnitude in all three cases. Since this emission comes from electron impact excitation of the ground state, the intensity rise indicates the drastic growth in the number of high energy electrons (with energies ≥23.07 eV). Obviously, this intensity rise is most pronounced in the case with the highest d*V*/d*t*. Another interesting observation is that the rise time of the emission intensity is ~0.7 ns, 1 ns, and 2 ns, respectively, which is very close to that of the discharge current (~0.5 ns, 0.7 ns, and 1.7 ns). This is because the excitation and ionization processes have very similar threshold energies (see figure 5(*c*)). In addition, both the emission intensity and the discharge current experience a 'phase transition': a fast increase during the breakdown phase and a slower increase in the second phase.

Figure 5(*b*) shows the temporal evolution of the He II 468.6 nm line (helium ion $n = 4 \rightarrow n = 3$). Similar to figure 5(*a*), the emission intensity of this ion line also has a sharp rise in the breakdown phase, indicating a continuous growth in the number of even higher energy electrons (with energies ≥75.60 eV). In the second phase (after ~1 ns when d*V*/d*t* is ~0.42 kV ns^{-1} for example), however, the rate of intensity increase is significantly lower. The reduction in this rate signifies a change in the excitation mechanism. In fact, in the second phase, with the increase in the density of electrons and metastable species, the stepwise processes start to play a major role for the excitation and ionization and the ground state excitation will no longer be the dominant process. This is because the high energy electrons are promptly relaxed due to the reduction of the driving force from the external electric field and the ever increasing electron–electron collisions. Even though this feature is present in the emission intensity from both the atom and the ion lines,

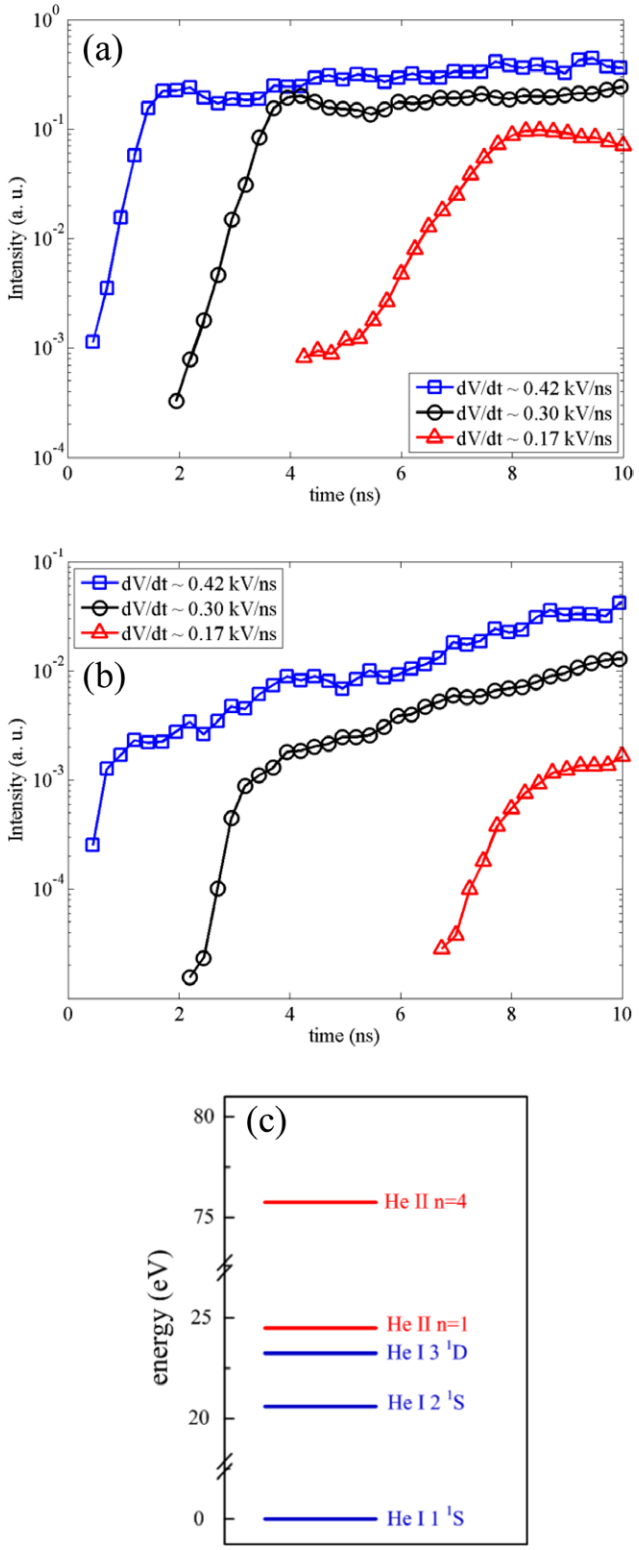

Figure 5. The temporal evolution of the He I 667.8 nm (*a*) and He II 468.6 nm (*b*) in different d*V*/d*t* cases. (*c*) shows a partial energy diagram of the helium atom and ion.

the ion line increases with a faster rate in this phase. This is because the ion line has two major sources of excitation: the excitation from the ground state ions and metastable atoms, while the atom line mainly comes from excitation from the metastable atoms. However, in order to have a quantitative description on the second phase, a model including all the stepwise processes should be developed, which is beyond the scope of this work.

4.3. The behavior of electrons in the breakdown phase

For the three discharges with different values of d*V*/d*t*, the breakdown process corresponds to the time period of ~0–1 ns, 2–3.5 ns, and 4–8 ns, respectively.

The breakdown phase is characterized by low electron density (estimated to be less than $10^{13}\,\mathrm{cm}^{-3}$), low metastable density, but a fast build-up of high energy electrons, indicated by a rising tail in the EEDF [13]. In this case, for both the ion and atom lines, the inelastic collision between the ground state atoms and high energy electrons is the dominant production process, as mentioned before. In fact, by analyzing the temporal evolution of both the ion and atom lines, some evidence of a rising tail in the EEDF can be found in the beginning period of the breakdown. Even though the threshold energy to excite the ion line is 75.60 eV and a much lower energy (23.07 eV) is needed for the helium atom line (figure 5(*c*)), the rise rate of the ion line emission tends to be higher than that from the atom (~5.9 GHz versus ~3.2 GHz when d*V*/d*t* is ~0.30 kV ns^{-1}) in the beginning period of the breakdown (~2–3 ns). Considering the energy dependence of the cross sections for these two processes [33, 34], a higher rise rate for the ion line suggests the prompt development of a high energy tail in the EEDF in the energy range of ~100 eV and above, at the beginning of the breakdown process.

According to the discussion above, one can estimate the temporal evolution of the excited state density in the breakdown phase by using a volume averaged rate balance equation. In fact, the spatial non-uniformity will not present a serious problem here, since the discharge seems to be quite uniform in the direction parallel to the electrode during the breakdown process (figure 3). In this equation, the production term is the excitation from the ground state helium atom and the major loss processes are dipole allowed transitions and quenching by atoms and electrons:

$$\frac{\mathrm{d}n_k}{\mathrm{d}t} = \int n_g \cdot \sigma_k(\boldsymbol{E}_e) \cdot \left(\frac{2\boldsymbol{E}_e}{m_e}\right)^{1/2} \cdot g_e(\boldsymbol{E}_e) \cdot \mathrm{d}\boldsymbol{E}_e - \left(A_k + Q_{a\ \mathrm{quench}\ k} \cdot n_g + Q_{e\ \mathrm{quench}\ k} \cdot n_e\right) \cdot n_k \tag{18}$$

where n_k is the number density of the excited state k for either the atom or the ion, n_g is the gas density, σ_k is the cross section by electron impact excitation for the excited state k, $\boldsymbol{E}_e$ is the electron energy, g_e is the EEDF, A_k is the Einstein coefficient of the excited state k and $Q_{a\ \mathrm{quench}\ k}$ and $Q_{e\ \mathrm{quench}\ k}$ are the quenching rate coefficient of the excited state k by atoms and electrons, respectively.

Dividing n_k on both sides of equation (18), we obtain:

$$\frac{\frac{\mathrm{d}n_k}{\mathrm{d}t}}{n_k} = \frac{\mathrm{d}\,In(n_k)}{\mathrm{d}t} = \frac{1}{n_k}\int n_g \cdot \sigma_k(\boldsymbol{E}_e) \cdot \left(\frac{2\boldsymbol{E}_e}{m_e}\right)^{\frac{1}{2}} \cdot g_e(\boldsymbol{E}_e) \cdot \mathrm{d}\boldsymbol{E}_e - (A_k + Q_{a\ \mathrm{quench}\ k} \cdot n_g + Q_{e\ \mathrm{quench}\ k} \cdot n_e) \tag{19}$$

Under the current experimental condition, the second term on the right hand side of equation (19) (the total loss rate) is estimated to be of the order of 100 MHz. On the other hand, from figure 5(*a*), one can estimate the emission intensity rise rate during the breakdown period, which varies between ~1.5 GHz and 4.9 GHz, depending on the value of d*V*/d*t*. The rise rate for the helium ion line is even higher than that of the atom line (figure 4(*b*)). Therefore,

$$\frac{\mathrm{d}\ \mathrm{In}(n_k)}{\mathrm{d}t} \gg \left(A_k + Q_{a\ \mathrm{quench}\ k} \cdot n_g + Q_{e\ \mathrm{quench}\ k} \cdot n_e\right) \tag{20}$$

Thus, the rate equation of these levels can be simplified as:

$$\frac{\Delta n_k}{\Delta t} \sim \frac{\mathrm{d}n_k}{\mathrm{d}t} = \int n_g \cdot \sigma_k(\boldsymbol{E}_e) \cdot \left(\frac{2\boldsymbol{E}_e}{m_e}\right)^{1/2} \cdot g_e\,(\boldsymbol{E}_e) \cdot \mathrm{d}\boldsymbol{E}_e \tag{21}$$

Apply equation(21) for these two lines and take the ratio, we obtain:

$$\frac{\Delta n_m}{\Delta n_n} = \frac{\int n_g \cdot \sigma_m(\boldsymbol{E}_e) \cdot \left(\frac{2\boldsymbol{E}_e}{m_e}\right)^{1/2} \cdot g_e\,(\boldsymbol{E}_e) \cdot \mathrm{d}\boldsymbol{E}_e}{\int n_g \cdot \sigma_n\left(\boldsymbol{E}_e\right) \cdot \left(\frac{2\boldsymbol{E}_e}{m_e}\right)^{1/2} \cdot g_e\,(\boldsymbol{E}_e) \cdot \mathrm{d}\boldsymbol{E}_e} = \frac{A_n}{A_m} \times \frac{\Delta I_m}{\Delta I_n} \tag{22}$$

where the relation:

$$I_k = A_k \cdot n_k \tag{23}$$

is used. Notice that equation (22) does not represent corona equilibrium since the breakdown is a fast transient process. In this case, the density of the excited species at a given time is given by the time integration of the term on the right hand side of equation (21). Equation (23) means that the emission intensity is in proportion with the instantaneous density of the excited states during the breakdown process. A change in the emission intensity reflects the change in the density of excited states. This is the reason why the temporal resolution of this optical emission spectroscopy method is not limited by the life time of excited species.

As these two lines have very different threshold energies (75.60 eV and 23.07 eV) and their cross sections have very different energy dependence, the relative distribution of the high energy electrons (weighted by the cross section) and its temporal evolution can be obtained from this ratio. Assuming a Maxwellian EEDF for this energy range, an 'effective electron temperature' (T_{eff}) can be obtained from equation (22), where ΔI is obtained from the difference of adjacent data points of the emission intensity. This parameter T_{eff} represents a 'local' slope of the EEDF in the energy region of tens to hundreds eV. The result is shown in figure 6.

It can be seen that the T_{eff} is very high (~33 eV) for the discharge with d*V*/d*t* ~ 0.42 kV ns^{-1}. This reveals the ability of the efficient generation of high energy electrons under high d*V*/d*t*, due to the intensified field at the ionization wave front when the breakdown happens. This result is consistent with these of the first (primary) streamer, where the electron temperature is the order of tens of eVs [29]. As shown in the experimental observation (figure 3) and modeling result (figure 4), the breakdown process evolves in a form of an ionization wave. Due to the limitation of experiment, the obtained T_{eff} is spatially averaged. The high energy electrons concentrate in the ionization wave front, where the electric field is high, while the low energy electrons have large population in the plasma column behind the ionization wave, where the electric field is low. Therefore, the electron energy in the ionization wave front should be much higher than the measured value. This argument is supported by the shape of the EEDF obtained from the Boltzmann equation, which shows an elevated tail (and even a plateau) up to ~800 eV during the breakdown process [13]. If the both peak voltage and the voltage rise rate are high enough, runaway electrons can be observed, as in [35, 36].

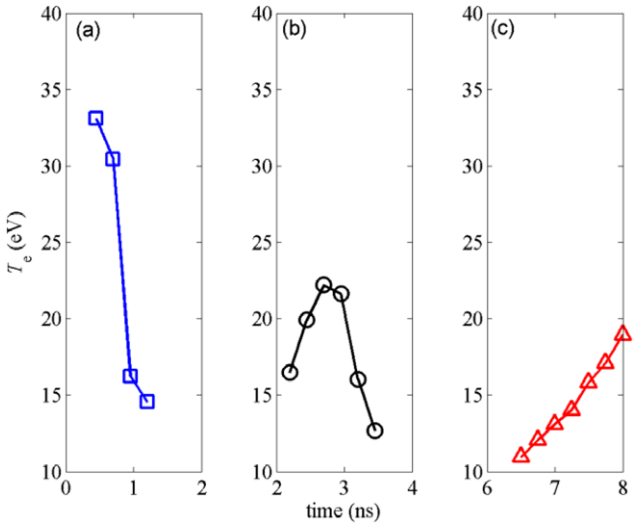

Figure 6. The temporal evolution of effective electron temperature (T_{eff}) with different values of d*V*/d*t*: (*a*) ~0.42 kV ns^{-1}, (*b*) ~0.30 kV ns^{-1}, and (*c*) ~0.17 kV ns^{-1}.

Furthermore, the breakdown phase can be divided into two 'sub-phases': a T_{eff} rising phase and a T_{eff} falling phase (a 'cooling' phase). This can be seen clearly in the d*V*/d*t* ~ 0.30 kV ns^{-1} case (figure 6(*b*)). In the first sub-phase, the density of electrons in the very tail of the EEDF increases much faster than that of the lower energy electrons. Therefore, the rise rate of the ion line is higher than that of the atom line, leading to an increase of T_{eff} in this first sub-phase. In the second sub-phase, these high energy electrons (with energies >75.60 eV) initiate intense ionization, resulting in a fast increase of the density of lower energy electrons. This leads to a decrease of the relative population of the high energy electrons and makes the T_{eff} drop (an apparent 'cooling'). Similar observation has been reported in [27]. However, in this sub-phase, the total number of high energy electrons keeps increasing, which is evidenced by the increasing emission intensity in the entire breakdown period. In the case of d*V*/d*t* ~0.42 kV ns^{-1}, however, the first sub-phase (and the increase of electron density) happens so fast that the current experimental setup cannot catch, so only the drop of T_{eff} can be seen (figure 6(*a*)). On the other hand, in the case of d*V*/d*t* ~ 0.17 kV ns^{-1}, the T_{eff} keeps increasing and no cooling is observed (figure 6(*c*)). This is because the magnitude of ionization is not strong enough (which can be seen from the much

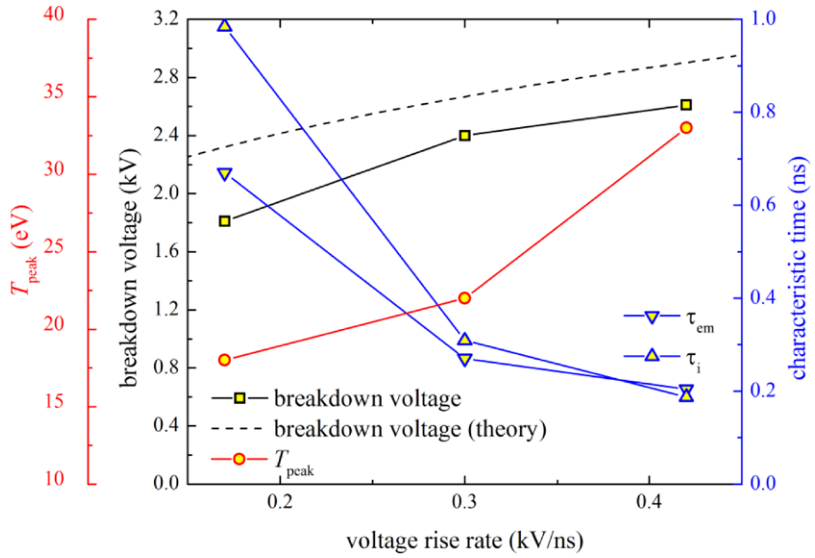

Figure 7. The relation between the breakdown voltage, the peak effective electron temperature during breakdown (T_{peak}), and the characteristic rise time of the emission intensity of He I 667.8 nm line (τ_{em}) and the discharge current (τ_i) during the breakdown period and the voltage rise rate. A relationship between the breakdown voltage and the voltage rise rate developed by a breakdown model in [24] is shown (dash line).

lower rise rate of the discharge current in this case), so the density of lower energy electrons cannot outgrow that of high energy electrons. However, after the breakdown process, the T_{eff} in this case should also decrease, as illustrated in [11].

In addition, as mentioned in section 4.1, the discharge current reflects the anisotropic part of the EVDF. The current can be considered as the product of the electron density, the cross section of discharge channel, and the electron drift velocity. The electron drift velocity under the peak electric field at the wave front is equal to the velocity of the ionization wave [26]. The mean velocity of the ionization wave can be estimated from the distance between the electrodes and the rise time of the discharge current. For discharges with dV/dt ~ 0.17 kV ns^{-1}, 0.30 kV ns^{-1}, and 0.42 kV ns^{-1}, this velocity corresponds to the electron energies of ~1 eV, 6 eV, and 18 eV, respectively. This rough estimation indicates that the electrons have a very anisotropic distribution during the breakdown process, especially for discharges with high dV/dt.

Figure 7 shows the relation between four discharge parameters and the voltage rise rate. The four parameters are the breakdown voltage, the peak effective electron temperature during breakdown (T_{peak}), and the characteristic time τ_{em} and τ_i. τ_{em} is defined as the reciprocal of the slope (in log scale) of emission intensity from the He I 667.8 nm line during the breakdown period, while τ_i is that of the discharge current. It can be seen that, when dV/dt increases from ~0.17 kV ns^{-1} to ~0.42 kV ns^{-1}, the breakdown voltage increases from ~1.8 kV to ~2.6 kV, which leads to the increase of T_{peak} from ~18 eV to ~33 eV. Even though the number of data is quite limited, T_{peak} seems to rise at a faster rate when dV/dt is high. This suggests the possibility of entering the runaway regime when dV/dt is ~0.42 kV ns^{-1}. In addition, both τ_{em} and τ_i drop fast with dV/dt, indicating the strong correlation between the rate of excitation and ionization with dV/dt, as mentioned before. Furthermore, when dV/dt is ~0.17 kV ns^{-1}, τ_{em} is smaller than τ_i. The reason may be that, with a relatively low T_{eff} in this case, the electrons favor excitation more than ionization, due to a lower value of threshold energy for excitation (figure 5(*c*)). However, when dV/dt increases, the difference between τ_{em} and τ_i is getting smaller. The possible explanation is, with the presence of electrons whose energies are tens of eV or higher, the effect of different threshold energies is no longer important.

4.4. Limitations

Both the measurement and modeling have some limitations. Due to the limited bandwidth of the measurement system and the presence of discharge jitter, the measured rise time of both the current and the emission intensity could be overestimated and the rise rate of these parameters could be underestimated. Another consequence of the limited temporal resolution is that, when dV/dt is ~0.42 kV ns^{-1}, the rising phase for the T_{eff} is not observed. Even though the discharge is quite uniform in the direction parallel to the electrodes, the discharge parameters can have a non-uniform distribution in the direction vertical to the electrodes. In addition, the T_{eff} is obtained by assuming a Maxwellian distribution for the energy range between tens and hundreds of eV. As for the limitation in the fluid model, even though the model can reveal the influence of the dV/dt on the most important features of the discharge during the breakdown process, the fluid approximation has yet to generate a satisfactory quantitative agreement with the experiment.

5. Conclusion

In this work, the influence of voltage rise rate on a nanosecond discharge in atmospheric pressure helium is investigated. The experiment is performed with a parallel-plate

discharge configuration. The voltage rise rate is varied between 0.17 kV ns^{-1} and 0.42 kV ns^{-1}. It is found that the rise rate of both the discharge current and the emission intensity increases drastically with the voltage rise rate. This demonstrates the remarkable capability of generating high energy electrons in the discharges with a high voltage rise rate. These arguments are supported by the increase in the measured effective electron temperature during the breakdown processes, namely ~18 eV when dV/dt is ~0.17 kV ns^{-1} and ~33 eV when dV/dt is ~0.42 kV ns^{-1}. Furthermore, the higher voltage rise rate results in a shorter rise time of both the discharge current and the emission intensity. Since the breakdown process evolves in a form of cathode directed ionization wave, a shorter rise time indicates faster propagation of the ionization wave. In addition, a simple fluid model is proposed and its predicted results agree reasonably well with the important discharge parameters measured in the experiment, such as the breakdown voltage and the rise rate and rise time of the discharge current.

Acknowledgment

This work is supported in part by the fund from Chinese Ministry of Science and Technology (Nos 2011ZX02403).

References

[1] Starikovskaia S M 2014 *J. Phys. D: Appl. Phys.* **47** 353001
[2] Adamovich I V, Choi I, Jiang N, Kim J-H, Keshav S, Lempert W R, Mintusov E, Nishihara M, Samimy M and Uddi M, 2009 *Plasma Sources Sci. Technol.* **18** 034018
[3] Starikovskii A Yu, Nikipelov A A, Nudnova M M and Roupassov D V 2009 *Plasma Sources Sci. Technol.* **18** 034015
[4] Rethmel C, Little J, Takashima K, Sinha A, Adamovich I V and Samimy M 2011 *AIAA 2011-487*
[5] Kakizaki K, Sasaki Y, Inoue T and Sakai Y 2006 *Rev. Sci. Instrum.* **77** 035109
[6] Treshchalov A B and Lissovski A A 2010 *Quantum Electron.* **40** 234
[7] Walsh J L and Kong M G 2007 *Appl. Phys. Lett.* **91** 251504
[8] Bruggeman P, Verreycken T, González M Á, Walsh J L, Kong M G, Leys C and Schram D C 2010 *J. Phys. D: Appl. Phys.* **43** 124005
[9] Warne L K, Jorgenson R E and Kunhardt E E 2014 *J. Appl. Phys.* **115** 143303
[10] Höft H, Kettlitz M, Becker M M, Hoder T, Loffhagen D, Brandenburg R and Weltmann K-D 2014 *J. Phys. D: Appl. Phys.* **47** 465206
[11] Huang B D, Takashima K, Zhu X M and Pu Y K, 2014 *J. Phys.* D*: Appl. Phys.* **47** 422003
[12] Nikandrov D S, Tsendin L D, Kolobov V I and Arslanbekov R R 2008 *IEEE Trans. Plasma Sci.* **36** 131
[13] Macheret S O, Shneider M N and Miles R B 2002 *IEEE Trans. Plasma Sci.* **30** 1301
[14] Komuro A, Ono R and Oda T 2013 *Plasma Sources Sci. Technol.* **22** 045002
[15] Yagi I, Okada S, Matsumoto T, Wang D, Namihira T and Takaki K 2011 *IEEE Trans. Plasma Sci.* **39** 2232
[16] Korolev Y D and Mesyats G A 1998 *Physics of Pulsed Breakdown in Gases* (Yekaterinburg: URO)
[17] Anikin N B, Pancheshnyi S V, Starikovskaia S M and Starikovskii A Yu 1998 *J. Phys. D: Appl. Phys.* **31** 826–33
[18] Huang B D, Zhu X M, Takashima K and Pu Y K 2013 *J. Phys.* D*: Appl. Phys.* **46** 464011
[19] Takashima K, Adamovich I V, Xiong Z, Kushner M J and Starikovskaia S 2011 *Phys. Plasmas* **18** 083505
[20] Nagaraja S, Yang V and Adamovich I V 2013 *J. Phys. D: Appl. Phys.* **46** 155205
[21] Wang Q, Economou D J and Donnelly V M 2006 *J. Appl. Phys.* **100** 023301
[22] Hagelaar G J M and Pitchford L C 2005 *Plasma Sources Sci. Technol.* **14** 722–33
[23] Bogdanov A, Kudryavtsev A A, Arslanbekov R R and Kolobov V I 2004 *J. Phys. D: Appl. Phys.* **37** 2987–95
[24] Levatter J I and Lin S C 1980 *J. Appl. Phys.* **51** 210
[25] Takashima K, Yin Z and Adamovich I V 2013 *Plasma Sources Sci. Technol.* **22** 015013
[26] Lagarkov A N and Rutkevich I M 1994 *Ionization Waves in Electrical Breakdown of Gases* (New York: Springer)
[27] Pancheshnyi S V, Starikovskaia S M and Starikovskii A Y 1999 *J. Phys. D: Appl. Phys.* **32** 2219–27
[28] Naĭdis G V 1997 *Pis'ma Zh. Tekh. Fiz.* **23** 89–94
[29] Ono R and Oda T 2003 *J. Phys. D: Appl. Phys.* **36** 1952–8
[30] Wang D, Namihira T and Akiyama H 2012 *Air Pollution—a Comprehensive Perspective*, ch 9 (Rijeka: InTech) www.intechopen.com/books/air-pollution
[31] Lieberman M A and Lichtenberg A J 2005 *Principles of Plasma Discharges and Materials Processing* 2nd edn, ch 14 (New York: Wiley)
[32] Raizer Y P 1992 *Gas Discharge Physics,* ch 12 (Berlin: Springer)
[33] Alves L L, Gousse G and Ferreira C M 1992 *J. Phys. D: Appl. Phys.* **25** 1713
[34] Bailey M, Bruch R, Rauscher E and Bliman S 1995 *J. Phys.* B*: At. Mol. Opt. Phys.* **28** 2655–69
[35] Yatom S, Vekselman V, Gleizer J Z and Krasik Ya E 2011 *J. Appl. Phys.* **109** 073312
[36] Tarasenko V F, Baksht E K, Erofeev M V, Kostyrya I D, Rybka D V and Shutko Y V 2013 *IEEE Trans. Plasma Sci.* **41** 2931